JACS
JOURNAL OF THE AMERICAN CHEMICAL SOCIETY

Article

pubs.acs.org/JACS

Rational Design of Selective Small-Molecule Inhibitors for β-Catenin/B-Cell Lymphoma 9 Protein−Protein Interactions

Logan R. Hoggard,[†] Yongqiang Zhang,[†] Min Zhang, Vanja Panic, John A. Wisniewski, and Haitao Ji*

Department of Chemistry, Center for Cell and Genome Science, University of Utah, Salt Lake City, Utah 84112-0850, United States

Supporting Information

ABSTRACT: Selective inhibition of α-helix-mediated protein−protein interactions (PPIs) with small organic molecules provides great potential for the discovery of chemical probes and therapeutic agents. Protein Data Bank data mining using the HippDB database indicated that (1) the side chains of hydrophobic projecting hot spots at positions *i*, *i* + 3, and *i* + 7 of an α-helix had few orientations when interacting with the second protein and (2) the hot spot pockets of PPI complexes had different sizes, shapes, and chemical groups when interacting with the same hydrophobic projecting hot spots of α-helix. On the basis of these observations, a small organic molecule, 4′-fluoro-*N*-phenyl-[1,1′-biphenyl]-3-carboxamide, was designed as a generic scaffold that itself directly mimics the binding mode of the side chains of hydrophobic projecting hot spots at positions *i*, *i* + 3, and *i* + 7 of an α-helix. Convenient decoration of this generic scaffold led to the selective disruption of α-helix-mediated PPIs. A series of small-molecule inhibitors selective for β-catenin/B-cell lymphoma 9 (BCL9) over β-catenin/cadherin PPIs was designed and synthesized. The binding mode of new inhibitors was characterized by site-directed mutagenesis and structure−activity relationship studies. This new class of inhibitors can selectively disrupt β-catenin/BCL9 over β-catenin/cadherin PPIs, suppress the transactivation of canonical Wnt signaling, downregulate the expression of Wnt target genes, and inhibit the growth of Wnt/β-catenin-dependent cancer cells.

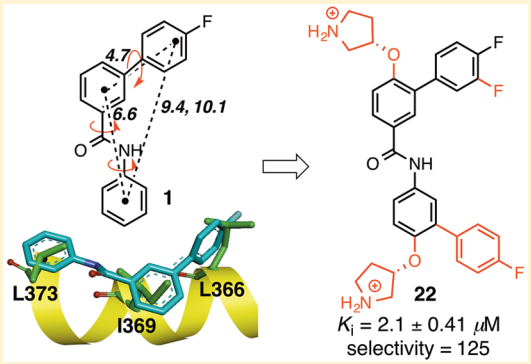

INTRODUCTION

Efficient targeting of protein−protein interactions (PPIs) with small organic molecules is a significant challenge.[1] Hot spots at PPI interfaces provide a starting point for designing PPI inhibitors.[2] However, how to achieve an efficient conversion of hot spot knowledge to a small-molecule inhibitor is an unsolved task.[3] For PPIs, the projecting hot spot of the ligand protein packs against the hot spot pocket of the target protein. The hot spot pocket of the target protein tends to undergo different induced-fit rearrangements when forming complex structures with different protein partners and small-molecule ligands.[2,4] Structure-based design of PPI inhibitors based only on the hot spot pocket(s) of the target protein can be challenging. We decided to analyze the orientations and chemical properties of the projecting hot spots of the ligand protein in the PPI structures. Small organic molecules (called fragments) were then designed to mimic the binding mode of projecting hot spots and used as the starting points for fragment-based inhibitor optimization. The role of α-helical peptides in mediating PPIs is well demonstrated.[5] For many α-helix-mediated PPIs, the side chains of the projecting hot spots of an α-helix appear at the same face and define the interacting surface for PPIs. We aimed to design a generic scaffold that itself can directly mimic the binding mode of the side chains of hydrophobic projecting hot spots at positions *i*, *i* + 3, and *i* + 7 of an α-helix. This generalized scaffold was then decorated for the selective disruption of specific protein−protein interfaces. Herein, we report one such scaffold and its application to generate selective inhibitors for the β-catenin/B-cell lymphoma 9 (BCL9) PPI, a key downstream effector of canonical Wnt signaling.

The canonical Wnt signaling pathway plays a critical role in embryonic development, cell proliferation, and tissue homeostasis.[6] β-Catenin is the primary mediator of this signaling pathway. The hyperactivation of canonical Wnt signaling leads to an accumulation of β-catenin in the cell nucleus. Nuclear β-catenin forms a supercomplex with T-cell factor (Tcf)/lymphoid enhancer-binding factor (Lef), BCL9/B9L (BCL9-like, a BCL9 paralogue), and CREB (cAMP response element-binding protein)-binding protein (CBP)/p300, etc. to activate the transcription of a number of β-catenin target genes including *AXIN2*, *LGR5*, *cyclin D1*, *c-myc*, and *LEF1*, which further promote cancer cell growth, migration, resistance to current drugs, and evasion from apoptosis. More importantly, canonical Wnt signaling is aberrantly overactivated in cancer stem cells, which drives cancer growth, seeds metastases, and causes cancer recurrence after remission. Significant efforts have been made to discover inhibitors for the canonical Wnt signaling pathway.[7] Formation of the β-catenin/BCL9 complex in the cell nucleus is the penultimate step of this signaling pathway. Transcriptional overactivation of canonical Wnt

Received: May 13, 2015
Published: September 9, 2015

ACS Publications © 2015 American Chemical Society

DOI: 10.1021/jacs.5b04988
J. Am. Chem. Soc. 2015, 137, 12249−12260

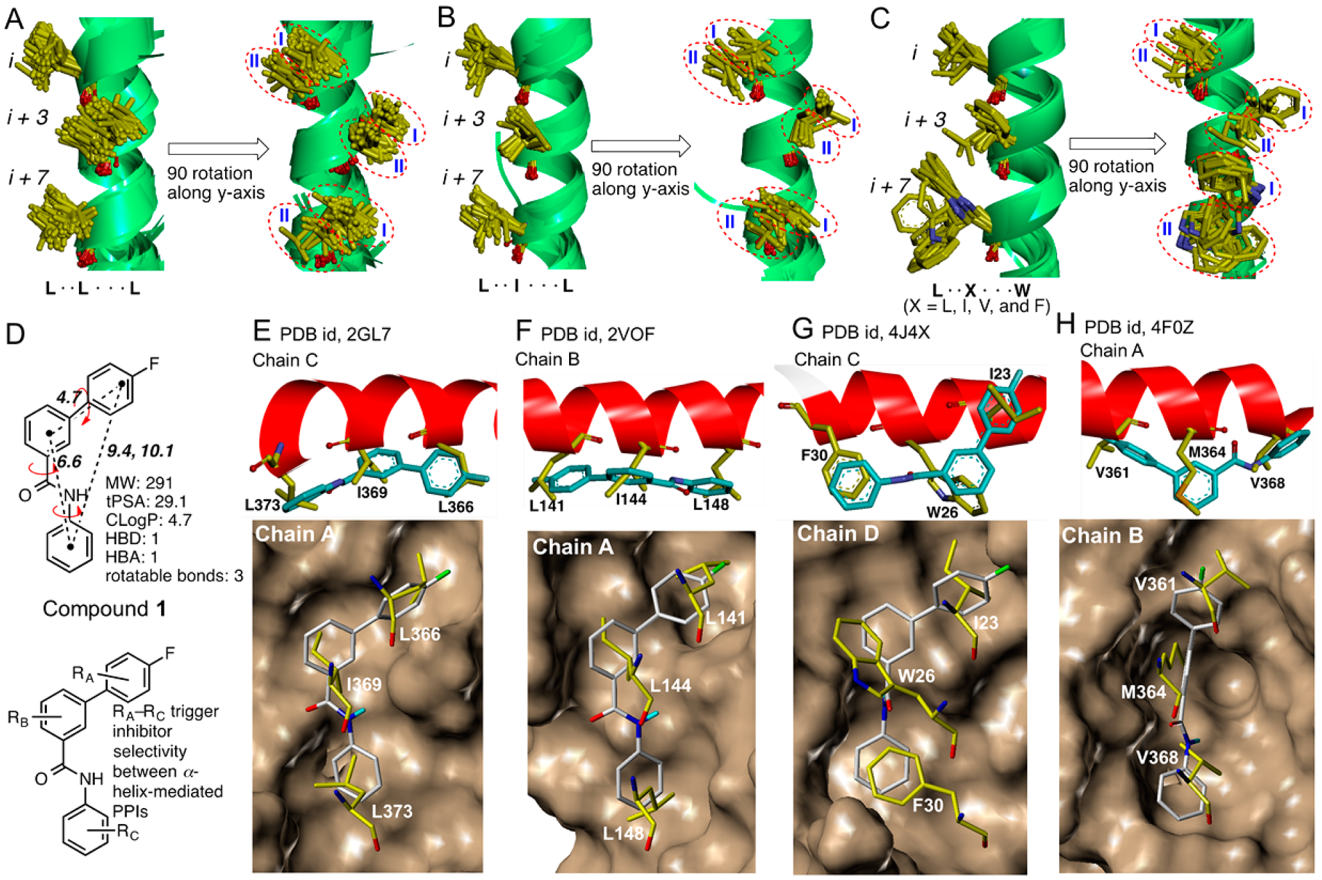

Figure 1. Design of a small-molecule scaffold that itself can directly mimic the binding mode of side chains of hydrophobic projecting hot spots at positions *i*, *i* + 3, and *i* + 7 of an α-helix. (A) Fifty-seven PPI structures that have projecting hot spots L••L•••L are rmsd-superimposed on the basis of backbone heavy atoms at positions *i*, *i* + 3, and *i* + 7. These 57 PPI structures are listed in Table S1. (B) Twenty-five PPI structures that have projecting hot spots L••I•••L, as shown in Table S1, are rmsd-superimposed on the basis of backbone heavy atoms at positions *i*, *i* + 3, and *i* + 7. (C) Twenty PPI structures that have projecting hot spots L••X•••W (X = L, I, V, and F, Table S1) are rmsd-superimposed on the basis of backbone heavy atoms at positions *i*, *i* + 3, and *i* + 7. (D) Chemical structure of **1**, 4′-fluoro-*N*-phenyl-[1,1′-biphenyl]-3-carboxamide. Distances between the centroids of each aromatic system are indicated in angstroms. Rotatable single bonds are indicated in red. MW, molecular weight; tPSA, topological polar surface area; clogP, calculated lipophilic coefficient; HBD, H-bond donor; and HBA, H-bond acceptor. (E) Compound **1** mimics the side-chain positioning of L366, I369, and L373 in human BCL9 (chain C) and is docked to human β-catenin (chain A). PDB id 2GL7.[14] (F) Compound **1** mimics the side-chain positioning of L141, I144, and L148 in mouse puma BH3 domain (chain C) and is docked into mouse prosurvival protein A1 (chain A). PDB id 2VOF.[27] (G) Compound **1** mimics the side-chain positioning of I23, W26, and F30 in protein N from Granada virus nucleocapsid (chain C) and is docked to protein N of Granada virus nucleocapsid (chain D). PDB id 4J4X.[28] (H) Compound **1** mimics the side-chain positioning of V361, M364, and V368 in calcineurin catalytic subunit (chain A) and is docked to the calcineurin regulatory subunit (chain B). PDB id 4F0Z.[29]

signaling is dependent on formation of the β-catenin/BCL9 complex, as evidenced by the upregulation of BCL9 and B9L in cancer cells[8−11] and the results from BCL9 or B9L knockdown[8−13] and dominant negative BCL9 or B9L[8,9] experiments. Crystallographic analysis reveals that homology domain 2 of BCL9 (residues S352−F374) adopts an α-helical structure to interact with the first armadillo repeat of β-catenin.[14] Stapled BCL9 L351−F374 α-helical peptides were designed to inhibit β-catenin/BCL9 PPIs.[15,16] Among them, SAH-BCL9$_B$ can pass the cell membrane, bind to β-catenin, disrupt β-catenin/BCL9 PPIs, and selectively suppress the transcription of Wnt target genes. This stapled peptide also inhibited cancer cell growth, angiogenesis, and metastasis without overt damage to normal tissues in the mouse xenograft models for colorectal carcinoma and multiple myeloma. The immunogenic effect and in vivo stability of this stapled α-helical peptide have not yet been reported. High-throughput screening (HTS) identified a small organic molecule, carnosic acid, that can disrupt the β-catenin/BCL9 PPI, inhibit β-catenin-dependent transcription, and destabilize activated β-catenin.[17] Carnosic acid is a natural antioxidant and associated with many biological activities. Its catechol substructure readily reacts with protein nucleophiles after oxidation and has been recognized as a substructure of pan assay interference compounds (PAINS).[18,19] This compound can be problematic in inhibitor optimization and biological studies. Therefore, there is an urgent need to develop class-specific small-molecule inhibitors for the β-catenin/BCL9 PPI.

RESULTS AND DISCUSSION

Rational Design of a Small-Molecule Scaffold to Mimic the Binding Mode of Side Chains of Hydrophobic Hot Spots at Positions *i*, *i* + 3, and *i* + 7 of an α-Helix. The helical PPI database HippDB[5,20−22] was interrogated to retrieve the protein−protein complexes that (1) are predicted to have hydrophobic projecting hot spots at positions *i*, *i* + 3, and *i* + 7 and (2) have concave pocket(s) on the second

DOI: 10.1021/jacs.5b04988
J. Am. Chem. Soc. 2015, 137, 12249−12260

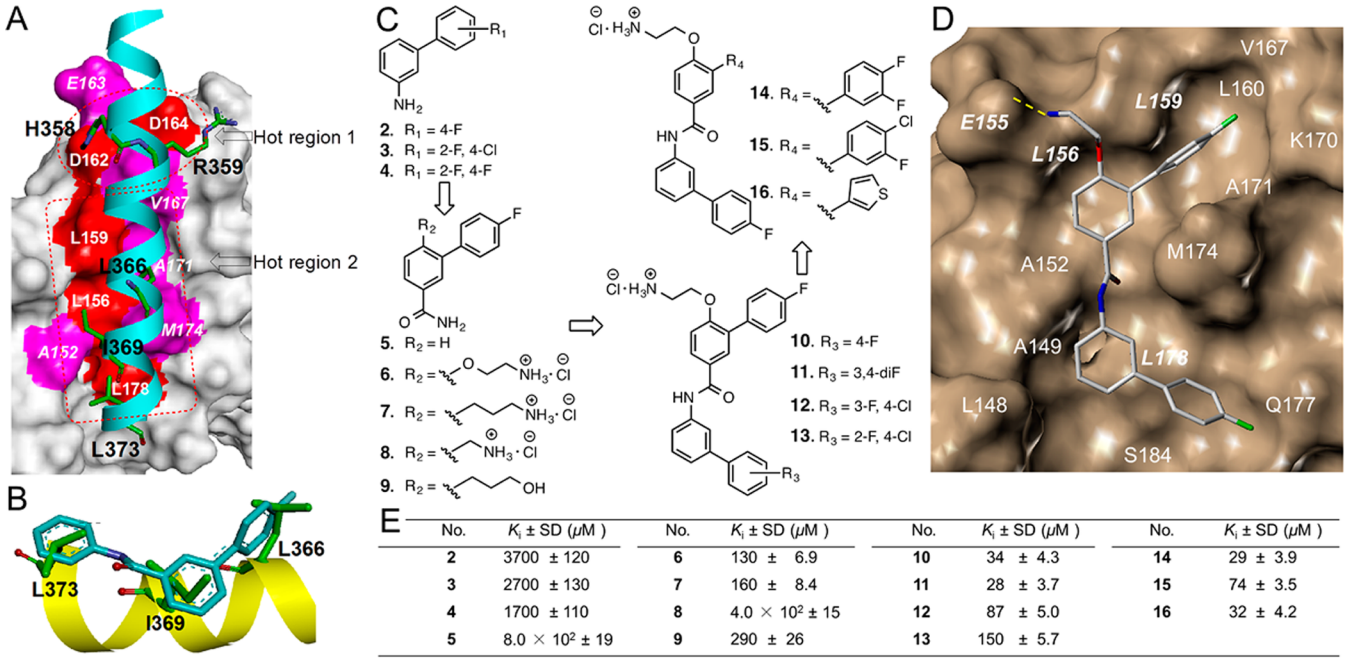

E

No.	K_i ± SD (μM)	No.	K_i ± SD (μM)	No.	K_i ± SD (μM)	No.	K_i ± SD (μM)
2	3700 ± 120	6	130 ± 6.9	10	34 ± 4.3	14	29 ± 3.9
3	2700 ± 130	7	160 ± 8.4	11	28 ± 3.7	15	74 ± 3.5
4	1700 ± 110	8	4.0×10^2 ± 15	12	87 ± 5.0	16	32 ± 4.2
5	8.0×10^2 ± 19	9	290 ± 26	13	150 ± 5.7		

Figure 2. Design of small-molecule β-catenin/BCL9 inhibitors. (A) Hot regions 1 and 2 for β-catenin/BCL9 PPIs. (B) Overlay of side chains of BCL9 residues L366, I369, and L373 with 4′-fluoro-*N*-phenyl-[1,1′-biphenyl]-3-carboxamide (**1**). (C) Chemical structures of **2**–**16**. (D) AutoDock result of **10** with β-catenin. A stick model of this docking result is shown in Figure S5. (E) AlphaScreen K_i values of **2**–**16**. Each set of data was expressed as mean ± standard deviation (n = 3). Details are shown in Figure S6.

protein to accommodate projecting hot spots. The analyzed hydrophobic residues of α-helices were leucine (L), isoleucine (I), methionine (M), valine (V), phenylalanine (F), and tryptophan (W). Out of 27 746 PPI entries in HippDB (on January 15, 2014), 733 PPI structures that meet these two criteria were retrieved and further superimposed by backbone heavy atoms at positions i, i + 3, and i + 7 of α-helices to minimize the root-mean-square deviation (rmsd). It was observed that side chains of the projecting hot spots of α-helices at the same position (i, i + 3, or i + 7) tended to be placed in limited spatial areas when forming the protein–protein complexes. Two main groups of spatial areas were identified for each of the three projecting hot spots, as shown in Figure 1A–C and Figure S1 in Supporting Information. Orientations I and II for hot spot i point away from and toward i + 3, respectively. Orientations I and II for hot spot i + 3 point toward i and i + 7; and orientations I and II for hot spot i + 7 point toward and away from i + 3. It was also noted that a small set of side chains of projecting hot spots F and W were not located in the areas for orientations I and II, and a detailed analysis of this set will be reported separately. A small-molecule scaffold, 4′-fluoro-*N*-phenyl-[1,1′-biphenyl]-3-carboxamide (**1**, Figure 1D), was then designed by a bioisostere-based fragment hopping protocol[23,24] to mimic the positioning of hydrophobic side chains of projecting hot spots with consideration of the sizes of hot spot pockets of the target protein, as well as the biocompatibility of newly generated ligand structures.[24−26] Three rotatable single bonds in **1** produce at least 16 low-energy conformations and allow good coverage of the conformational space as described in Supporting Information. The extensive HippDB data mining indicated that **1** mimicked 86% PPIs that had such hydrophobic projecting hot spots from α-helices and concave pockets from the target proteins (631 out of 733 structures, Table S1). Two side-chain patterns that were difficult for scaffold **1** to mimic are orientation I (i)–orientation II (i + 3)–orientation II (i + 7) and orientation I (i)–orientation II (i + 3)–orientation II (i + 7). Eighteen protein–protein complexes of these 631 structures, whose disruption potentially has important biomedical applications, were selected as the examples. Four examples are shown in Figure 1E–H, and 14 other examples are described in Figure S2. Based on the structure of **1**, substituents R_A–R_C in Figure 1D can be introduced to trigger inhibitor selectivity because the structural features that differentiate α-helix-mediated PPIs can reside in the protein–protein interfaces adjacent to the hot spot pockets, as observed by comparison of the 18 protein–protein complexes in Figure 1E–H and Figure S2.

Design of β-Catenin/BCL9 Inhibitors Based on Scaffold 1. Crystallographic and biochemical analyses revealed two hot regions at the β-catenin/BCL9 interface (Figure 2A).[9,14,30−33] In hot region 1, residues D162, E163, and D164 of human β-catenin form an acidic knob[30] and interact with residues H358 and R359 of human BCL9. The D162A mutation of β-catenin reduced its binding with BCL9.[30] β-Catenin mutation D164A abrogated the interaction with BCL9 or B9L in vitro[31] and BCL9-dependent Wnt transcription in vivo.[32] Mutation of residues H358 or R359 of BCL9 to alanine significantly reduced its interaction with β-catenin.[14] The ^{358}HRE^{360}/^{358}AKQ^{360} mutation of BCL9 completely disrupted its binding with β-catenin.[9] In hot region 2, residues L366, I369, and L373 of BCL9 interact with a hydrophobic pocket that is lined with residues L159, V167, L160, A171, M174, L178, A149, A152, and L156 of β-catenin. BCL9 mutations L366K,[9] L373A,[9] and L366A/I369A[14] prevented its binding with β-catenin in the pulldown experiment. A similar result was also observed in the cell-based study. BCL9 mutant L366K and B9L mutant L411K could not coimmunoprecipitate with β-catenin.[9] BCL9 mutations L366A, I369A, and L373A had no observable inhibition of wild-type β-catenin/wild-type BCL9 PPIs in the fluorescence polarization (FP) competitive

DOI: 10.1021/jacs.5b04988
J. Am. Chem. Soc. 2015, 137, 12249–12260

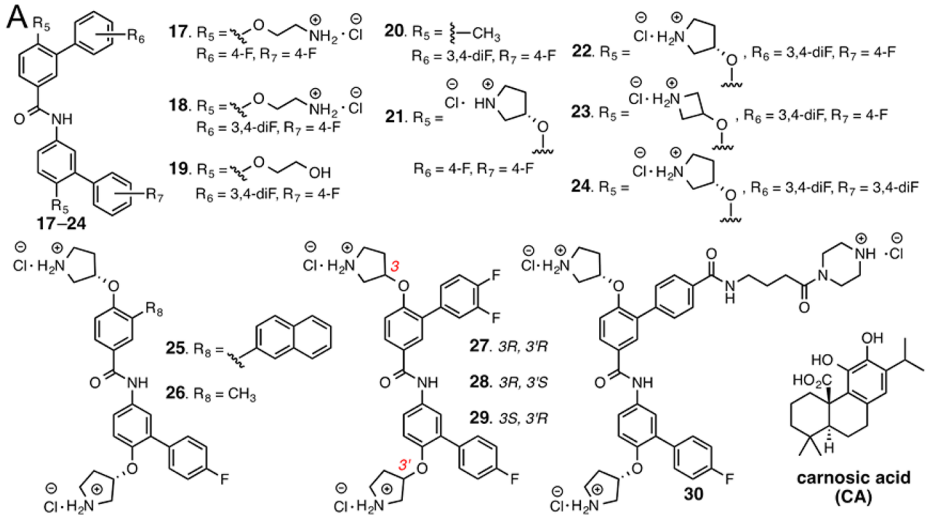

C

No.	K_i ± SD (μM) β-catenin/BCL9	K_i ± SD (μM) β-catenin/E-cadherin	selectivity BCL9/cadherin
17	12 ± 1.3	–	–
18	6.1 ± 1.5	230 ± 8.7	38
19	37 ± 2.7	–	–
20	4.0 × 10² ± 16	–	–
21	6.7 ± 0.78	230 ± 14	35
22	2.1 ± 0.41	260 ± 7.8	125
23	17 ± 2.0	270 ± 12	16
24	8.7 ± 0.89	260 ± 11	30
25	370 ± 15	–	–
26	2.0 × 10² ± 9.3	–	–
27	4.1 ± 0.36	210 ± 7.0	52
28	6.0 ± 0.51	110 ± 5.8	19
29	3.4 ± 0.35	140 ± 9.2	40
30	2.1 ± 0.43	720 ± 20	345
CA	5.3 ± 0.80	390 ± 16	73

D

β-catenin	K_d (μM)	ΔH (cal/mol)	ΔS (cal/mol•K)
Wild type	0.33 ± 0.010	–1900 ± 24	23 ± 0.090
D145A/E155A	3.2 ± 0.15	–3.0 × 10² ± 20	24 ± 0.11
L159S	0.92 ± 0.033	–970 ± 50	24 ± 0.18
L156S/L178S	1.59 ± 0.045	–620 ± 25	24 ± 0.10

E

β-catenin	K_i ± SD (μM) 18	21	22
Wild type	6.1 ± 1.5	6.7 ± 0.78	2.1 ± 0.41
D145A	28 ± 2.4	29 ± 2.6	13 ± 1.7
E155A	29 ± 2.6	31 ± 2.1	13 ± 1.8
D145A/E155A	160 ± 5.0	150 ± 9.2	97 ± 7.8

Figure 3. Optimization of new β-catenin/BCL9 inhibitors. (A) Chemical structures of **17**–**30**. (B) AutoDock result of **22** with β-catenin. A stick model of this docking result is shown in Figure S7. (C) AlphaScreen K_i values of **17**–**30** and carnosic acid (CA) for β-catenin/BCL9 PPIs and AlphaScreen K_i values of **18**, **21**–**24**, **27**–**30**, and CA for β-catenin/E-cadherin PPIs. Each set of data was expressed as mean ± standard deviation (n = 3). Details are shown in Figures S8 and S9. (D) ITC results of **22** with wild-type and mutant human β-catenin (residues 138–686). Details are shown in Figure S10. The K_i value of **22** from the AlphaScreen assay (2.1 ± 0.41 μM) is 6.3-fold higher than that from the ITC experiment (0.33 ± 0.0010 μM). The high concentrations of β-catenin (7.5–10 μM) and small-molecule inhibitors (75–100 μM) used in the ITC studies might also contribute to the lower ITC K_d value. (E) AlphaScreen competitive inhibition assay results of **18**, **21**, and **22** for disruption of wild-type β-catenin/wild-type BCL9 and mutant β-catenin/wild-type BCL9 PPIs. Each set of data was expressed as mean ± standard deviation (n = 3). Details are shown in Figure S11.

inhibition assay.[33] The pulldown experiment showed that β-catenin mutants L159A and L178A bound with BCL9; however, a double mutation, β-catenin L156A/L159A, abolished its interaction with BCL9.[14] Our site-directed mutagenesis experiments demonstrated that β-catenin mutations L156S or L159S reduced the binding affinity with BCL9, while β-catenin mutations D145A, E155A, and D145A/E155A had no effect on β-catenin/BCL9 PPIs. β-Catenin double mutations L156S/L159S and L156S/L178S abolished binding with BCL9 (results are shown in Figures S3 and S4).

An overlay of scaffold **1** with BCL9 residues L366, I369, and L373 is shown in Figures 1E and 2B. To verify this design, compounds **2**–**16** in Figure 2C were synthesized (synthetic routes for **2**–**16** are shown in Schemes S1–S6). Compounds **2**–**5** were designed to mimic the binding mode of the side chains of L366 and I369. The AlphaScreen assay[34] showed that these compounds inhibited the β-catenin/BCL9 PPI at a low millimolar range (Figure 2E). A 4-aminoethoxy or 4-aminopropyl side chain was introduced to **5** with an attempt to form charge–charge and H-bond interactions with E155. The AlphaScreen assay showed that the resulting compounds, **6** and **7**, were 5-fold more potent than **5**. The one-carbon-shorter derivative **8** and the hydroxyl derivative **9** were less potent than **7**, probably due to weakened electrostatic interactions. Compounds **10**–**13** were designed to explore the pocket adjacent to β-catenin L178. The *para* and *meta* positions of the terminal benzene ring of the biphenyl-3-amino moiety can tolerate fluorine substitution. Compounds **14**–**16** were designed to optimize the interactions with residues L159, L160, V167, and A171. The results showed that 4-fluoro and 3,4-difluoro derivatives **10** and **14** exhibited higher potency than **15**. On the other hand, the 3-thionyl derivative **16** had a similar potency as **10**. An AutoDock[35] docking result for **10** is shown in Figure 2D.

Structure–Activity Relationship-Based Hit Optimization. Compounds **17**–**29** in Figure 3A were designed to generate more potent β-catenin/BCL9 inhibitors (synthetic routes for **17**–**29** are shown in Schemes S7–S11). A second aminoethoxy group was introduced to **10** and **14** to produce additional charge–charge and H-bond interactions with β-catenin D145. As shown in Figure 3C, **17** and **18** were more potent than **10** and **14**. Compounds **19** and **20** were designed to explore the role of β-catenin D145 and E155 in inhibitor binding. Compound **19** was predicted to have H-bonds but no charge–charge interactions with D145 and E155, while **20** lost both H-bond and charge–charge interactions. The AlphaScreen assay showed that **19** and **20** were 6- and 65-fold less potent than **18**, respectively. The (*S*)-pyrrolidin-3-yloxy group of **21**

DOI: 10.1021/jacs.5b04988
J. Am. Chem. Soc. 2015, 137, 12249–12260

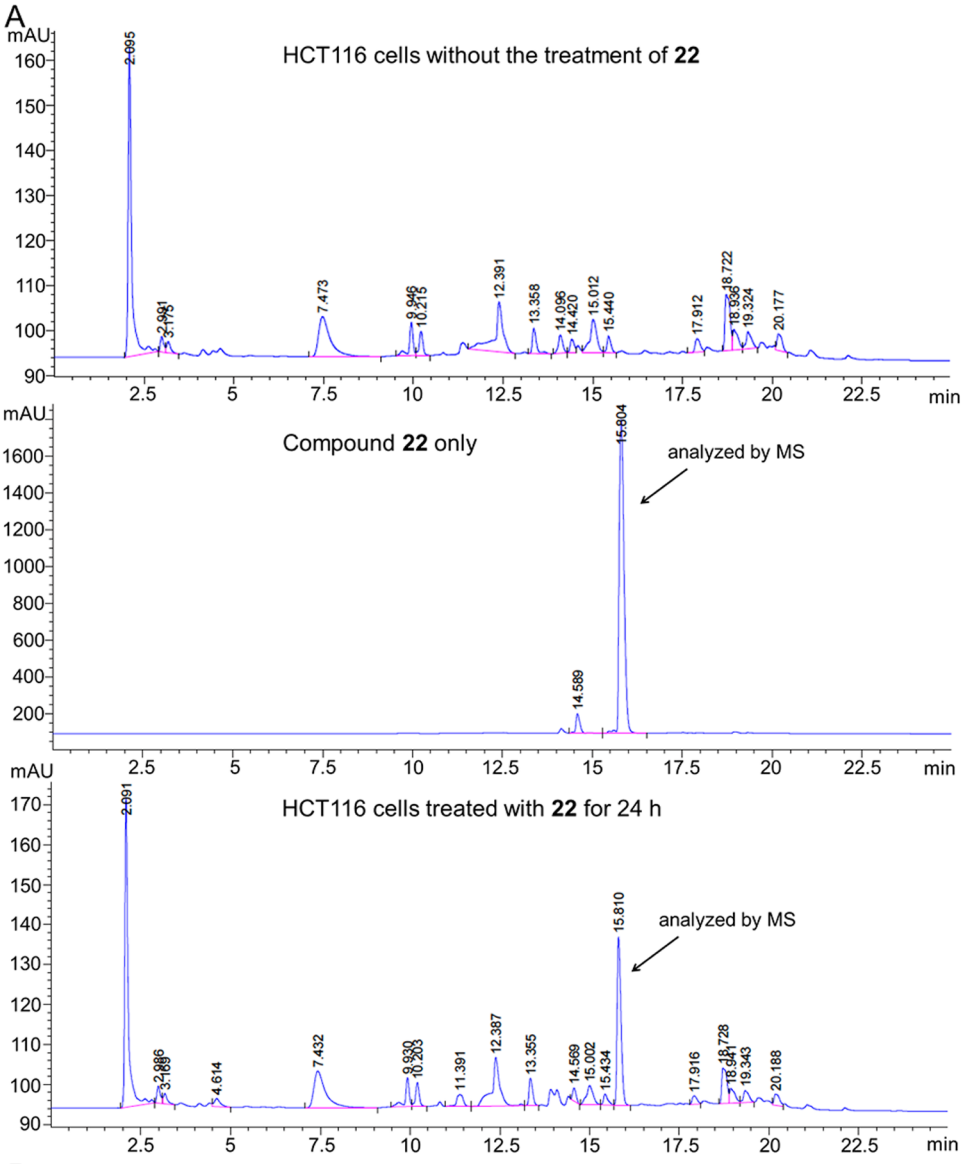

B

	Physical Properites							IC_{50} ± SD (μM)		
No.	MW	HBD	HBA	tPSA	rotatable bonds	cLogP	$logD_{7.4}$	Wnt-activated HEK293	SW480	MDA-MB-231
10	445	2	2	64.4	7	5.58	3.95	38 ± 6.9	–	–
21	557	3	3	71.6	8	5.01	2.53	15 ± 1.5	9.7 ± 0.87	8.0 ± 1.1
22	575	3	3	71.6	8	5.08	2.57	4.5 ± 1.3	2.9 ± 0.33	3.4 ± 0.71
23	547	3	3	71.6	8	5.06	2.78	25 ± 5.6	21 ± 5.0	–
CA	331	4	2	77.8	2	3.67	0.407	–	5.2 ± 0.60	–

Figure 4. Cellular uptake and inhibition of Wnt activation by new β-catenin/BCL9 inhibitors. (A) HPLC-UV chromatograms of the studied samples. HCT116 colon cancer cells were used. The HPLC retention time of **22** was 15.8 min. MS data for pure and intracellular **22** are shown in Figure S14. Details to derive the intracellular concentration of **22** are shown in Figure S15 and described in the Experimental Procedures section. (B) Physical properties and Wnt-responsive luciferase reporter assay results for **10**, **21**–**23**, and carnosic acid. Details are given in Figure S16. Each set of data is expressed as mean ± standard deviation (n = 3).

and **22** was designed to replace the aminoethoxy group of **17** and **18** in an attempt to increase the cellular permeability. These two compounds were 2–3-fold more potent than **17** and **18**, respectively, likely due to the conformational constraint of the five-membered ring. Compound **22** exhibited a K_i value of 2.1 ± 0.41 μM and was more potent than carnosic acid in the parallel assay. Both AutoDock and Glide[36] docking studies predicted the same binding mode for **22**, as shown in Figure 3B. Substitution of the pyrrolidine ring of **22** with an aziridine ring led to a decrease in inhibitory activity. Derivative **24** has the 3,4-difluoro substituent on both terminal benzene rings, exhibiting slightly lower potency than **21**. Replacement of the 3,4-difluorophenyl group of **22** with a 2-naphthyl or methyl group drastically decreases its inhibitory potency, projecting the size of the hot spot pocket. The other three stereoisomers of **22** were also synthesized. The AlphaScreen assay of **27**–**29** indicated that these three stereoisomers had similar inhibitory activities as **22**. This result is consistent with that predicted from the AutoDock studies because D145 and E155 are located

DOI: 10.1021/jacs.5b04988
J. Am. Chem. Soc. 2015, 137, 12249–12260

on the surface of the ligand binding pocket and can access to the pyrrolidine nitrogen atoms of all studied stereoisomers.

Isothermal Titration Calorimetry and Site-Directed Mutagenesis Studies. An isothermal titration calorimetry (ITC) study showed that **22** bound wild-type β-catenin but not BCL9 (Figure S10). The trend of K_d values for **10** and **22** from the ITC studies was consistent with that observed from the AlphaScreen assay. The K_d value of **22** with β-catenin double mutant D145A/E155A was 9.6-fold higher than that with wild-type β-catenin (Figure 3D), implicating the importance of the side chains of D145 and E155 for inhibitor binding. The K_d values of **22** with β-catenin mutants L159S and L156S/L178S were 0.92 ± 0.033 and 1.6 ± 0.045 μM, respectively, further validating the proposed binding mode. Since neither D145A nor E155A affects the β-catenin/BCL9 PPI, as demonstrated by AlphaScreen competitive binding and fluorescence anisotropy binding assays (Figures S3 and S4), additional AlphaScreen competitive inhibition assays were performed to evaluate the effects of these mutations on K_i values of **18**, **21**, and **22**. As shown in Figure 3E, the K_i values of **22** for β-catenin D145A/BCL9 and β-catenin E155A/BCL9 PPIs were 13 ± 1.7 and 13 ± 1.8 μM, respectively, indicating that the side-chain carboxylic groups of D145 and E155 in β-catenin were important for inhibiting potency. The deletion of both side-chain carboxylic groups of D145 and E155 led to a further reduction of inhibitory activity. The K_i value of **22** was 97 ± 7.8 μM for β-catenin D145A/E155A double mutant/BCL9 PPIs. The same trend in K_i value changes was also observed for **18** and **21** (Figure 3E).

Inhibitor Selectivity Studies. β-Catenin has two functions in cells. One is interaction with Tcf/Lef, BCL9/B9L, CBP/p300, etc., in the cell nucleus to culminate in canonical Wnt signaling. The second is interaction with cadherin to fulfill its function for cell−cell adhesion. Crystallographic analyses reveal that the β-catenin/BCL9 PPI interface was also used to bind region V of E-cadherin.[14,37] Two key residues of murine E-cadherin, F871 and L874 (PDB id 1I7W), occupy the same positions as human BCL9 residues L366 and I369 (PDB id 2GL7) and project to the same hot spot pocket of β-catenin (Figure S12). This overlap presents a potential risk that β-catenin/BCL9 inhibitors might disrupt β-catenin-mediated cell−cell adhesion, although the β-catenin/E-cadherin PPI has a much larger contact surface than the β-catenin/BCL9 PPI. AlphaScreen selectivity assays were used to evaluate the selectivity of **18**, **21**−**24**, and **27**−**29** between β-catenin/BCL9 and β-catenin/E-cadherin PPIs. As shown in Figure 3C, all tested β-catenin/BCL9 inhibitors can selectively target β-catenin/BCL9 over β-catenin/E-cadherin PPIs. Among them, **22** exhibited 125-fold selectivity and was more selective than carnosic acid in the parallel assay. It should be noted that the K_d value for the β-catenin/BCL9 PPI (280−710 nM)[14,34] is higher than that for the β-catenin/E-cadherin PPI (41−82 nM).[34,38−40] Inhibitor selectivity may be partially owing to the weaker interaction between β-catenin and BCL9. Noting that hot region 1 in Figure 2A is used to bind BCL9 but not E-cadherin, we designed and synthesized compound **30** to form charge−charge and H-bond interactions with D164 (Figure S13 and Scheme S12). The AlphaScreen assay showed that this compound exhibited comparable inhibitory potency for β-catenin/BCL9 PPIs as **22**. However, it exhibited much higher selectivity for β-catenin/BCL9 over β-catenin/E-cadherin PPIs, underscoring the future direction for inhibitor optimization.

The derived K_i values of small-molecule inhibitors are much lower for β-catenin/BCL9 PPI than for β-catenin/E-cadherin PPIs. These results seemingly contradict the definition of K_i, for which a competitive inhibitor should have the same value regardless of the identities and concentrations of the competing ligands. We believe that this difference in K_i values of PPI inhibitors comes from different contact surface areas and hot regions between protein−protein complexes. For example, crystallographic analysis indicated that the surface area for β-catenin/E-cadherin PPIs was extensive and had five regions.[37] Only region V overlaps with that for β-catenin/BCL9 PPIs.[14] The mechanism of partial inhibition by the concentrations of inhibitors used in the biochemical assays is likely different between β-catenin/BCL9 and β-catenin/E-cadherin PPIs, resulting in the different K_i values. More analysis will be required to fully understand this difference. Experimental IC_{50} values are also provided in Figure S9 for comparison.

Cellular Uptake and Inhibition of β-Catenin/BCL9/Tcf Transcriptional Activity. To determine whether new β-catenin/BCL9 inhibitors can be taken up by Wnt/β-catenin-dependent cancer cells, an HPLC/MS analysis was conducted to measure the concentration of **22** in HCT116 colon cancer cells. HCT116 cells were first treated with 2 μM **22** for 24 h. Intracellular **22** was then successfully separated from the other cellular components by HPLC (Figure 4A) and characterized by MS (Figure S14). Further quantification concluded that the concentration of **22** in HCT116 cells was 1.66 ± 0.0286 μM (83% cellular retention ratio; Figure S15). It is noted that this cellular uptake assay relies on extraction of larger numbers of cells (1.7×10^6) and cannot determine the concentration of inhibitor in specific subcellular compartments. To determine whether new β-catenin/BCL9 inhibitors can inhibit the transactivation of canonical Wnt signaling, Wnt-responsive luciferase reporter assays were performed with Wnt-activated human embryonic kidney cell line 293 (HEK293), colorectal cancer cell line SW480, and triple-negative breast cancer cell line MDA-MB-231. As shown in Figure 4B, **10** and **21**−**23** can effectively inhibit the activity of TOPFlash luciferase (luciferase reporter with wild-type Tcf4 binding sites) without reducing absolute Renilla values (internal controls) and affecting the activity of FOPFlash luciferase (luciferase reporter with mutant Tcf4 binding sites).

Inhibition of Expression of Wnt/β-Catenin Target Genes. *AXIN2*, *LGR5*, *cyclin D1*, and *LEF1* are target genes for the canonical Wnt signaling pathway. *AXIN2* is a specific target gene for this signaling pathway. *LGR5* is a marker for intestinal stem cells. *Cyclin D1* and *LEF1* are upregulated in many cancer cells and promote tumorigenesis. Real-time quantitative polymerase chain reaction (PCR) experiments were performed to evaluate the effects of new β-catenin/BCL9 inhibitors on the mRNA levels of these Wnt target genes. As shown in Figure 5A, **22** downregulated the transcription of *AXIN2*, *LGR5*, *LEF1*, and *cyclin D1* in dose-dependent manners in MDA-MB-231 cells. More than 50% of mRNA expression was inhibited at doses of 2 and 4 μM of **22**. Dose-dependent inhibition of mRNA expression of Wnt target genes was also observed for SW480 cells (Figure S17). Protein expression levels of cyclin D1, c-Myc, the active form of β-catenin (ABC),[41] and total β-catenin in SW480 cells were examined by Western blot analysis (Figure 5B). Protein expression levels of cyclin D1 and c-Myc were significantly reduced after treatment with **22**. Compound **22** reduced activated β-catenin in the cell nucleus but had no effect on E-cadherin-bound β-catenin,

DOI: 10.1021/jacs.5b04988
J. Am. Chem. Soc. 2015, 137, 12249−12260

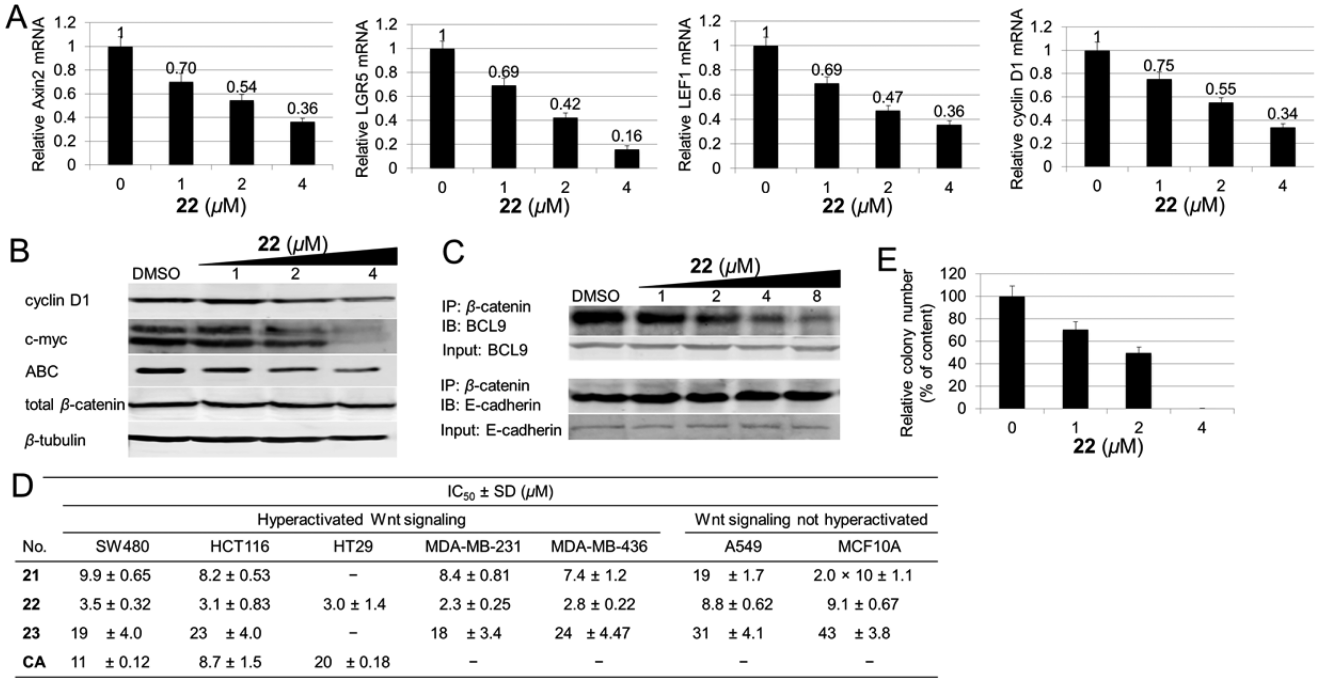

D

	IC_{50} ± SD (μM)						
	Hyperactivated Wnt signaling					Wnt signaling not hyperactivated	
No.	SW480	HCT116	HT29	MDA-MB-231	MDA-MB-436	A549	MCF10A
21	9.9 ± 0.65	8.2 ± 0.53	–	8.4 ± 0.81	7.4 ± 1.2	19 ± 1.7	2.0 × 10 ± 1.1
22	3.5 ± 0.32	3.1 ± 0.83	3.0 ± 1.4	2.3 ± 0.25	2.8 ± 0.22	8.8 ± 0.62	9.1 ± 0.67
23	19 ± 4.0	23 ± 4.0	–	18 ± 3.4	24 ± 4.47	31 ± 4.1	43 ± 3.8
CA	11 ± 0.12	8.7 ± 1.5	20 ± 0.18	–	–	–	–

Figure 5. Further cell-based studies of new β-catenin/BCL9 inhibitors. (A) Quantitative real-time PCR study to determine changes in mRNA expression of *AXIN2*, *LGR5*, *LEF1*, and *cyclin D* in MDA-MB-231 cells in response to different concentrations of **22**. Each set of data is expressed as mean ± standard deviation (n = 3). (B) Western blot analysis to monitor the change of protein expression of cyclin D1, c-myc, ABC, and total β-catenin in response to different concentrations of **22** in SW480 cells. β-Tubulin was used as an internal reference. Experiments were performed in duplicate. (C) Coimmunoprecipitation experiments to evaluate the selectivity of **22** for β-catenin/BCL9 over β-catenin/cadherin PPIs in HCT116 cells. IP, immunoprecipitation; IB, immunoblotting; input, 10% amount of cell lysate. Experiments were performed in duplicate. (D) MTS tetrazolium assay to monitor the effects of **21**–**23** and carnosic acid (CA) on growth of SW480, HCT116, HT29, MDA-MB-231, MDA-MB-436, A549, and MCF10A cells. Each set of data is expressed as mean ± standard deviation (n = 3). (E) Inhibition of anchorage-independent growth of **22** in HCT116 cells. Details are given in Figure S19.

indicating that **22** does not inhibit the upstream sites of canonical Wnt signaling. Dose-dependent inhibition of mRNA and protein expression was also observed for **23**, as shown in Figure S18.

Cell-Based Inhibitor Selectivity and Inhibition of Viability for Wnt/β-Catenin-Dependent Cancer Cells. Coimmunoprecipitation experiments were performed to evaluate inhibitor selectivity in a cellular context. As shown in Figure 5C, **22** inhibited the β-catenin/BCL9 PPI in a dose-dependent manner. A parallel experiment indicated that **22** had no effect on the β-catenin/E-cadherin PPI at concentrations that were sufficient to inhibit the β-catenin/BCL9 PPI. MTS tetrazolium cell viability assays were performed to assess the effect of β-catenin/BCL9 inhibitors on growth of colorectal cancer cells (SW480, HCT116, and HT29) and triple-negative breast cancer cells (MDA-MB-231 and MDA-MB-436), all of which have hyperactivated Wnt signaling (Figure 5D). The MTS assay results showed that **21**–**23** inhibited cell growth in dose-dependent manners. Compounds **21** and **22** were more potent than carnosic acid and exhibited higher cytotoxicity for Wnt signaling-activated cells over Wnt signaling-latent cells, such as lung adenocarcinoma cell line A549 and normal mammary epithelial cell line MCF10A. As shown in Figure 5E, **22** inhibited the anchorage-independent growth of SW480 cells in a dose-dependent manner.

Comparison with Related Studies. Several approaches, such as hydrocarbon-stapled α-helices,[42] covalent hydrogen-bond mimetics,[43] and helical foldamers using β-peptides,[44] have been reported to stabilize a short peptide into a helical conformation for the inhibition of native PPIs. Terphenyl derivatives are small organic molecules that can mimic one face of an α-helical peptide.[45] The substituents on the terphenyl scaffold can occupy the area where the side chains of α-helical residues i, i + 3/4, and i + 7 are located. Some terphenyl derivatives have been reported as new inhibitors for Bcl-xL/Bak[46,47] and MDM2/p53[48] PPIs. A number of other small molecules that can mimic α-helical residues at positions i, i + 3/4, and i + 7 were also reported including terpyridines,[49] pyridazines,[50] dipiperazinobenzenes,[51] oxopiperazines,[52] terphthalamides,[53] benzoylureas,[54] benzamides and trisbenzamides,[55−57] trispyridylamides,[58,59] pyrrolopyrimidines,[60] and triazines.[61] All of these α-helix mimetics use rigid or preorganized scaffolds to overlap with the backbone of α-helices and then position three substituents in the area where the side chains of residues i, i + 3/4, and i + 7 are located.[62] Projecting hot spots at positions i, i + 3/4, and i + 7 of α-helices could be the primary driving force for many other PPIs and protein folding. The installation of functional groups to trigger inhibitor selectivity/specificity and maintain druglike properties has not been an easy task for the above-mentioned α-helix mimetics, with few successful examples reported.[48,63] HTS identified that nutlin[64] and benzodiazepinedione[65] can mimic F19 (i), W23 (i + 4), and L26 (i + 7) of an α-helix of p53 for disruption of the MDM2/p53 PPI. In a separate study, oxindole was designed to mimic the side chain of W23 in p53, and two hydrophobic substituents were introduced to the spirooxindole core to mimic the binding mode of the side chains of F19 and L26 of p53.[66] All of these compounds were designed for inhibition of MDM2/p53 PPIs and have not been generalized to other PPI interfaces. An anthraquinone scaffold was designed

DOI: 10.1021/jacs.5b04988
J. Am. Chem. Soc. 2015, 137, 12249−12260

to mimic the sagittal axis of an α-helix. The substituents on this scaffold were then used to mimic the binding mode of projecting hot spots L62 (i), I65 (i + 3), and D67 (i + 5) of Bim BH3 domain for dual inhibition of the Bcl-2/Bim and Mcl-1/Bim PPIs.[67] The quinone substructure in the anthraquinone scaffold can be reactive and has also been recognized as a PAINS substructure.[18,19] Semirigid scaffolds that can express hot spot side chains have been used to mimic the backbones of α-helices and explore key orientations at the PPI interfaces to generate new inhibitors for unexplored PPIs.[68] This study highlighted the importance of mimicking key side chains at the protein−protein interfaces.

Our PDB data mining based on the HippDB database indicated that (1) the side chains of hydrophobic projecting hot spots at positions i, i + 3, and i + 7 of an α-helix were placed in common spatial areas when they interacted with the second protein and (2) the hot spot pockets of different PPI complexes had different sizes, shapes, and chemical groups when they interacted with the same hydrophobic projecting hot spots at positions i, i + 3, and i + 7 of α-helix. On the basis of these observations, 4′-fluoro-*N*-phenyl-[1,1′-biphenyl]-3-carboxamide **1** was designed as a generic scaffold that itself directly mimics the binding mode of the side chains of hydrophobic projecting hot spots at positions i, i + 3, and i + 7 of an α-helix. Decoration of this generic scaffold could lead to small-molecule inhibitors that selectively disrupt α-helix-mediated PPIs. A series of selective small-molecule inhibitors for β-catenin/BCL9 PPIs including **22** was developed, based on scaffold **1**. It is worth noting that scaffold **1** does not contain the exact structures of α-helical side chains. Instead, it is a binding mode mimic and serves as a starting point for the design of selective small-molecule inhibitors for specific PPIs.

CONCLUSION

The discovery of a selective inhibitor for helix-mediated PPIs is challenging. The side chains of hydrophobic projecting hot spots of an α-helix are oriented to limited spatial areas when it interacts with the second protein. This observation provides an opportunity to design small-molecule inhibitors to mimic the binding mode of the side chains of α-helix hot spots and generate selective PPI inhibitors with high ligand efficiency. In this study, compound **1** in Figure 1D was designed as a generic scaffold that simultaneously mimic the hydrophobic interaction of side chains of hot spots at positions i, i + 3, and i + 7 of an α-helix. PDB data mining indicated that this scaffold can mimic 86% of 733 PPIs in the HippDB database that have predicted hydrophobic projecting hot spots with this pattern and concave pockets in the interacting protein. This scaffold enables the design of selective small-molecule inhibitors for helix-mediated PPI targets, because the sites that trigger PPI selectivity often exist adjacent to hot spot pockets where the projecting hot spots interact.

The β-catenin/BCL9 PPI is a key downstream effector of canonical Wnt signaling. Previous crystallographic and biochemical studies revealed that BCL9 S352−F374 adopts an α-helix structure to interact with the first armadillo repeat of β-catenin with L366 (i), I369 (i + 3), and L373 (i + 7) of BCL9 as the projecting hot spots. Based on the structure of **1**, a small-molecule inhibitor for β-catenin/BCL9 PPIs, **22** in Figure 3A, was designed and synthesized. In the design of **22**, two positively charged pyrrolidino groups and a substituted phenyl ring are introduced to scaffold **1** to trigger inhibitor selectivity between α-helix-mediated PPIs. The binding mode of **22** was then evaluated by structure−activity relationship and site-directed mutagenesis studies by use of two orthogonal assays, AlphaScreen and ITC. Cell-based studies demonstrated that **22** can inhibit the transactivation of canonical Wnt signaling, selectively disrupt β-catenin/BCL9 over β-catenin/cadherin PPIs in biochemical and cell-based assays, downregulate Wnt target genes, and inhibit the growth of cancer cells with hyperactivated Wnt signaling. HPLC/MS analysis showed that **22** was effectively taken up by HCT116 cells. The inhibitory activities of **22** and **23** (a structurally similar but less potent analogue) are consistent in biochemical and cell-based assays, indicating a specific inhibition of canonical Wnt signaling. All these data indicate that ***22** represents the first class-specific small-molecule inhibitor for β-catenin/BCL9 PPIs reported to date*. Further optimization based on **22** will lead to potent and selective chemical probes for the β-catenin/BCL9 PPI and potentially a new class of drug candidates for the treatment of advanced cancers. Compared to scaffold **1**, the two positively charged pyrrolidino rings and the additional phenyl ring in **22** likely resulted in this compound and its derivatives acting as specific β-catenin/BCL9 inhibitors in cell-based studies. Future studies will include optimization of inhibitors; determination of the β-catenin structure in complex with a small-molecule inhibitor (no such structure has been reported yet); application of scaffold **1** to other PPI interfaces in which the α-helical partners also have hydrophobic projecting hot spots at positions i, i + 3, and i + 7; and design of new inhibitor scaffolds that can simultaneously mimic the binding mode of three projecting hot spots of α-helices.

EXPERIMENTAL PROCEDURES

Protein Structure for Computer Modeling. Crystallographic coordinates for human β-catenin (PDB id 2GL7, 2.60 Å resolution, R_{cryst} = 0.223) were obtained from the Research Collaboratory for Structural Bioinformatics (RCSB) Protein Data Bank (PDB). Preparation of the crystal structure and molecular modeling were achieved with the commercially available Schrodinger (http://www.schrodinger.com/), BIOVIA Discovery Studio 3.0 (http://accelrys.com/), and SYBYL X2.0 (http://www.tripos.com/) software packages. The missing side chains of β-catenin were added in SYBYL X2.0. Protonation states of the residues were set to pH 7.0 when hydrogen was added. The AMBER 7 force field 99 and the AMBER FF99 charges within SYBYL X2.0 were used to optimize the orientation of hydrogen atoms and the missing side chains of the protein. After the protein complex was optimized, chains B (Tcf4), C (BCL9), D (second monomer of β-catenin), E (second monomer of Tcf4), F (second monomer of BCL9), and solvent molecules were removed, leaving only one monomer of β-catenin for further calculation. Residues in the BCL9 L366/I369/L373 binding site of β-catenin include D144−A146, L148, A149, A152, I153, E155−L160, D162−A171, M174, V175, Q177, L178, K180, K181, A183, S184, A187, I188, M194, and I198.

Fragment Hopping to Design 4′-Fluoro-*N*-phenyl-[1,1′-biphenyl]-3-carboxamide as a Binding Mode Mimic for Hydrophobic Side Chains of α-Helical Hot Spots *i*, *i* + 3, and *i* + 7. The stepwise protocol for fragment hopping was described previously.[23,24] Crystallographic coordinates for human β-catenin (PDB id 2GL7) were used in fragment design. The side chains of three projecting hot spots of BCL9, L366, I369, and L371, were identified as the critical binding elements to mimic. The BCL9 L366/I369/L373 binding site of β-catenin was defined as the hot spot pocket to accommodate the designed fragment. The hydrophobic side chains that defined the hot spot pocket were L148, A149, A152, L156, L159, L160, V167, K170, A171, M174, and L178 of β-catenin. The basic fragment library[23] and the bioisostere library[23] were interrogated to identify new fragments that can match the proposed critical binding elements.

DOI: 10.1021/jacs.5b04988
J. Am. Chem. Soc. 2015, 137, 12249−12260

Table 1

peptide	sequence[a]
BCL9 26-mer	H-^{350}GLSQEQLEHRERSLQTLRDIQRMLFP^{375}-NH_2
biotinylated BCL9 26-mer	biotin-Ahx-^{350}GLSQEQLEHRERSLQTLRDIQRMLFP^{375}-NH_2
FITC-labeled BCL9 26-mer	FITC-Ahx-^{350}GLSQEQLEHRERSLQTLRDIQRMLFP^{375}-NH_2
biotinylated E-cadherin 54-mer	biotin-^{824}APPYDSLLVFDYEGSGSEAASLSSLNSSESDKDQDYDYLNEWGNRFKKLADMYG^{877}-NH_2

[a]Ahx = 6-aminohexanoic acid.

Table 2

mutant	primer 1	primer 2
D145A	ggcagaccatcatcgcgttcttataattattg	aattataagaacgcgatgatggtctgccaag
E155A	ctggtcagatgagcaagagcacagatg	catctgtgctcttgctcatctgaccag
L156S	gtgcaatccctgaatcgacaaaactgctaaatg	catttagcagttttgtcgattcagggattgcac
L159S	ctgaactgacaaaatcgctaaatgacgaggac	gtcctcgtcatttagcgattttgtcagttcag
L156S/L159S	ctgaatcgacaaaatcgctaaatgacgaggac	gtcctcgtcatttagcgattttgtcgattcag
L178S	gttatggtccatcagtcttctaaaaaggaagcttc	gaagcttccttttagaagactgatggaccataac

The binding modes of new fragments were generated by fragment docking with AutoDock 4.2. Only the polar hydrogen atoms were kept on the protein structure, and the Kollman united atom charges were assigned. The grid maps were calculated by use of AutoGrid with grid spacing of 0.375 Å. For fragment docking, any atoms within 6 Å of the above critical binding elements were used to define the grid box, which resulted in two pockets: one pocket included side chains of A152, L156, L159, L160, V167, K170, A171, and M174 of β-catenin and side-chain carboxylic oxygens of E155 and D162 of β-catenin; while the second pocket included side chains of L148, A149, A152, M174, and L178, side-chain NH_3^+ of K181, side-chain OH of S184, backbone NH of A183, side-chain carboxylic oxygen atoms of D145 and S184, and backbone carbonyl oxygen of L148 of β-catenin. Docking was performed by use of the Lamarckian genetic algorithm, and the pseudo-Solis and Wets method was applied for the local search. Each docking experiment was performed 50 times, yielding 50 docked conformations. The other settings were standard default parameters. Results of the docking experiments were evaluated by auxiliary clustering analysis and visual inspection to match the proposed binding elements. Binding poses of the fragments that matched the proposed binding elements were stored in a SYBYL molecular database.

The distance between each fragment of two pockets was measured, and the linkers in the linker library[23] were merged to generate the ligand structure. Synthetic accessibility of the generated compounds was evaluated with the assistance of SciFinder. The generated ligand scaffolds were then docked in the binding site and visually inspected. If the newly generated ligand scaffold did not match the proposed critical binding elements, the ligand scaffold was rejected, and new structures were constructed by repeating the above steps. If the binding mode of the new ligand scaffold matched the proposed critical binding elements, they would be kept for further evaluation. The rules for metabolic stability[23] and the toxicophore library[23] were used to evaluate biocompatibility of the acceptable ligand scaffolds.

Ligand Docking by Use of Glide 5.8. The Glide grid box was defined to include all residues of the BCL9 L366/I369/L373 binding site. Default parameters were used to generate the receptor grid. The standard precision (SP) mode was used in ligand docking. The ligand scaling factor was set to 0.5 for atoms with partial charges lower than 0.15. The number of poses per ligand for the initial phase of docking was increased to 10 000. The 1000 best poses per ligand were kept for energy minimization, with a maximum number of minimization steps of 5000. A maximum of 100 000 ligand poses per docking run and 50 poses per ligand were collected. Up to 100 poses per ligand were kept for postdocking minimization. Default settings were used for the remaining parameters.

Ligand Docking by Use of AutoDock 4.2. Three-dimensional (3D) structures of the ligands were built, and the partial atomic charges were calculated by the Gasteiger−Marsili method. Rotatable bonds in the ligands were defined by use of AutoTors, which also united the nonpolar hydrogens and partial atomic charges to the bonded carbon atoms. The grid maps were calculated by use of AutoGrid. The AutoDock area was defined to include all residues in the BCL9 L366/I369/L373 binding site, and the grid spacing was set to 0.375 Å. Docking was performed by use of the Lamarckian genetic algorithm, and the pseudo-Solis and Wets method was applied for the local search. Each docking experiment was performed 100 times, yielding 100 docked conformations. The other settings were default parameters. All ligands followed the same docking protocol. Results of the docking experiments were evaluated by auxiliary clustering analysis and visual inspection to match the proposed critical binding elements.

Syntheses of 2−30. Synthetic procedures for **2**−**30** are given in Supporting Information.

Protein Expression and Purification. β-Catenin and its mutants (residues 138−686) were cloned into a pET-28b vector carrying a C-terminal 6× histidine tag (Novagen) and transformed into *Escherichia coli* BL21 DE3 (Novagen). Cells were cultured in Luria−Bertani (LB) medium with 30 μg/mL kanamycin until OD_{600} was approximately 0.8, and then protein expression was induced with 400 μM isopropyl β-D-1-thiogalactopyranoside (IPTG) at 20 °C overnight. Cells were lysed by sonication. Proteins were purified by nickel−nitrilotriacetic acid (Ni-NTA) affinity chromatography (30210, Qiagen) and dialyzed against a buffer containing 20 mM Tris (pH 8.5), 100 mM NaCl, 10% glycerol, and 3 mM dithiothreitol (DTT). The purity of β-catenin was greater than 95% as determined by sodium dodecyl sulfate (SDS)−polyacrylamide gel analysis. Native nondenaturing gel electrophoresis was performed to confirm the homogeneity of the purified proteins. Thermal-shift assay was performed on an iCycler iQ real-time detection system (Bio-Rad) to monitor protein stability and detect protein aggregation. Protein unfolding was evaluated through measuring the fluorescence changes of fluorescent dye Sypro Orange when interacting with wild-type or mutant β-catenin proteins. A temperature increment of 1 °C/min was applied. All proteins were stable and no aggregation was observed under storage or assay conditions. Proteins were aliquoted and stored at −80 °C.

BCL9 Peptide Synthesis and Purification. Human BCL9 (residues 350−375), *N*-terminally biotinylated human BCL9 (residues 350−375), *N*-terminally fluorescein-labeled human BCL9 (residues 350−375), and *N*-terminally biotinylated human E-cadherin (residues 824−877) were synthesized by InnoPep Inc. (San Diego, CA; www.innopep.com). All synthesized peptides were purified by HPLC with purity >95%. The structures were validated by LC/MS. The sequences are given in Table 1.

Site-Directed Mutagenesis Experiments. β-Catenin mutants D145A, E155A, L156S, L159S, D145A/E155A, L156S/L159S, and L156S/L178S were generated by the overlapping PCR method. Template for the mutagenesis reactions was wild-type full-length β-catenin in pET-28b. KOD hot start DNA polymerase (Novagen) was

DOI: 10.1021/jacs.5b04988
J. Am. Chem. Soc. 2015, 137, 12249−12260

Table 3Primer pairs for qPCR[71,72]

human gene	forward primer	reverse primer
GAPDH	5′-GAAGGTGAAGGTCGGAGTC-3′	5′-GAAGATGGTGATGGGATTTC-3′
AXIN2	5′-AGTGTGAGGTCCACGGAAAC-3′	5′-CTTCACACTGCGATGCATTT-3′
LGR5	5′-TGCTGGCTGGTGTGGATGCG-3′	5′-GCCAGCAGGGCACAGAGCAA-3′
LEF1	5′-GACGAGATGATCCCCTTCAA-3′	5′-AGGGCTCCT GAGAGGTTTGT-3′
cyclin D1	5′-ACAAACAGATCATCCGCAAACAC-3′	5′-TGTTGGGGCTCCTCAGGTTC-3′

used through this experiment. Mutants were confirmed by direct sequencing (Core facility, University of Utah). Following confirmation of the sequence, mutant β-catenin was cloned into a pET-28b vector and transformed into *E. coli* BL21 DE3. Primers for site-directed mutagenesis are given in Table 2.

The primers to produce β-catenin fragments (residues 138−686) from full-length β-catenin are forward, 5′-GGGGGGTCATGAT-CAACTTGATTAACTATCAAG-3′, and reverse, 5′-AAAACCCTC-GAGCTCTGTTCTGAAGAGAG-3′.

AlphaScreen Competitive Inhibition Assays Using Wild-Type and Mutant β-Catenin Proteins. Experimental details of the AlphaScreen competitive inhibition assays for β-catenin/BCL9 and β-catenin/E-cadherin PPIs have been described previously.[34] Concentrations of mutant β-catenin proteins used in the AlphaScreen competitive inhibition assays were the same as that of wild-type β-catenin protein.

Isothermal Titration Calorimetry Experiments. ITC measurements were performed at 28 °C on a VP-ITC instrument (Microcal, GE Healthcare Life Sciences). Wild-type and mutant β-catenin proteins were concentrated to 7−10 μM in buffer A [20 mM Tris, pH 8.8, 100 mM NaCl, 1 mM tris(2-carboxyethyl)phosphine (TCEP), and 8% glycerol]. Compounds **10** and **22** were set to 70−100 μM in buffer A depending upon the concentrations of β-catenin proteins used (compound concentrations were 10 times higher than those of proteins). The homogeneity of purified proteins was examined by native gel electrophoresis. Each titration experiment was initiated by a 2 μL injection and followed by 30−35 injections with an 8 μL volume each. Blank titrations, which were carried out by injecting the compound into the buffer, were subtracted from each data set. Association constant K_A, enthalpy change ΔH, and stoichiometry N were obtained from fitting the data by use of the Origin software package. Dissociation constant K_d, free energy change ΔG, and entropy change ΔS were obtained from basic thermodynamic equations: $K_d = K_A^{-1}$, $\Delta G = -RT \ln K_A$, and $\Delta G = \Delta H - T\Delta S$.

Intracellular HPLC/MS Analysis.[69,70] Colon cancer HCT116 cells with 0.7×10^6 density were seeded into a T-25 flask. Cell culture medium was Dulbecco's modified Eagle's medium (DMEM) with 10% fetal bovine serum (FBS). When cells reached approximately 70% confluency, the culture medium was removed, and **22** was added into new medium (DMEM with 10% FBS). The final concentration of **22** was 2 μM, and the final concentration of dimethyl sulfoxide (DMSO) was 0.02% (v/v). Cells further grew at 37 °C in a CO_2 incubator for 24 h. Control samples, which contained HCT116 cells with 0.02% (v/v) DMSO in medium but without **22**, were routinely prepared. After incubation, the medium was removed, and 1.7×10^6 cells were washed twice quickly with cold phosphate-buffered saline (PBS). Next, 1.5 mL of cold acetonitrile/methanol (1:1 v/v) was added to denature cellular proteins and to extract the compound. Extraction of samples was allowed to progress to completion by storing overnight at 4 °C. After thorough mixing, the samples were centrifuged in sealed 1.5 mL centrifuge tubes at 12 500 *g* for 15 min at 4 °C. The supernatant fraction was decanted into a glass tube and evaporated to dryness in a rotary evaporator. The sample was used immediately or stored at −20 °C.

For HPLC analysis, a Kromasil 300−5-C18 column (4.6 × 250 nm) was used. Injection volumes were 10 μL for pure **22** and 20 μL for cell samples. The HPLC flow rate was 1.5 mL/min, and UV detection at 254 nm was used. Gradient elution was applied: 100% H_2O (0.1% trifluoroacetic acid, TFA) for 6 min; 100% H_2O (0.1% TFA) to H_2O (0.1% TFA)/MeCN = 50/50 from 6 to 15 min; H_2O (0.1% TFA)/MeCN = 50/50 to 100% MeCN from 15 to 18 min; and 100% MeCN from 18 to 25 min. The retention time of **22** was 15.8 min. MS data were recorded by a Waters TQD Acquity instrument with an electrospray ionization (ESI) source.

A calibration curve was prepared with pure **22** to correlate the HPLC areas under the curve (AUCs) with concentrations of **22**, as shown in Figure S15. Two to three HPLC injections were conducted for each compound concentration. The intracellular volume was determined by measuring the pellet volume of 1.7×10^6 HCT116 cells. Experiments were preformed in triplicate. The resulting cell volume was 9.5 ± 0.2 μL. To determine the intracellular concentration of **22**, the dried cell sample was diluted in 200 μL of deionized (DI) water, and 20 μL of the sample was analyzed by HPLC as described above. The intracellular concentration of **22** was calculated by use of the calibration equation given in Figure S15 as follows:

$$[\mathbf{22}]_{\text{intracellular}} = \frac{[\mathbf{22}]_{\text{calibration eq}}}{2} \times \frac{200}{9.5}$$

Cell Transfection and Luciferase Reporter Assay. FuGENE6 (E269A, Promega) 96-well plate format was used for transfection of HEK293, SW480, and MDA-MB-231 cells according to the manufacturer's instructions. HEK293 cells were cotransfected with 45 ng of TOPFlash (or FOPFlash) reporter gene, 135 ng of pcDNA3.1−β-catenin, and 20 ng of pCMV-RL normalization reporter gene. SW480 and MDA-MB-231 cells were cotransfected with 60 ng of TOPFlash or FOPFlash reporter gene and 40 ng of pCMV-RL normalization reporter. Cells were cultured in DMEM and 10% FBS at 37 °C for 24 h, and different concentrations of inhibitors or DMSO were added. After 24 h, luciferase reporter activity was measured by use of the Dual-Glo system (E2940, Promega). Normalized luciferase activity in response to treatment with **10**, **21**−**23**, and carnosic acid was compared with that obtained from cells treated with DMSO. Experiments were performed in triplicate.

Quantitative Real-Time Polymerase Chain Reaction Analysis. SW480 and MDA-MB-231 cells at 1×10^6/mL were treated with different concentrations of **22** and **23** for 24 h. Total RNAs were extracted with TRIzol (15596026, Life Technologies), and cDNA was synthesized with the Superscript III first-strand kit (18080-051, Invitrogen). Quantitative polymerase chain reaction (qPCR) was performed by use of the iQ SYBR green supermix kit (170-8880, Bio-Rad) on an iQ^5 multicolor real-time PCR reaction system (Bio-Rad). The threshold cycle (C_T) values were normalized to that of internal reference *GAPDH*. The primer pairs are listed in Table 3. Experiments were performed in triplicate.

Western Blotting. SW480 cells at 1×10^6 cells/mL were treated with different concentrations of **22** and **23** for 24 h. Cells were lysed in buffer containing 50 mM Tris (pH 7.4), 150 mM NaCl, 1% Nonidet P-40, 0.5% sodium deoxycholate, 0.1% SDS, and protease inhibitors. After centrifugation at 12 000 rpm for 20 min at 4 °C, the supernatant was loaded onto an SDS−8% polyacrylamide gel for electrophoretic analysis. Separated proteins were transferred onto nitrocellulose membranes for immunoblot analysis. Antibodies against total β-catenin (610153, BD Biosciences, most of which is phosphorylated β-catenin and represents the E-cadherin-bound pool), active form of β-catenin (ABC, 05-665, EMD Millipore, dephosphorylated at positions S37 and T41 of β-catenin),[41] cyclin D1 (sc-853, Santa Cruz Biotechnology, Inc.), c-Myc (D84C12, Cell Signaling), and β-tubulin (sc-55529, Santa Cruz Biotechnology, Inc.) were incubated with the membranes overnight at 4 °C. IRDye 680LT goat anti-mouse IgG (827-11080, LiCOR) or IRDye 800CW goat anti-rabbit IgG (827-

DOI: 10.1021/jacs.5b04988
J. Am. Chem. Soc. 2015, 137, 12249−12260

08365, LiCOR) was used as the secondary antibody. Images were detected by the Odyssey infrared imaging system (LiCOR). Experiments were performed in duplicate.

Coimmunoprecipitation Assay. HCT116 cells at 1×10^6/mL were treated with different concentrations of **22** for 24 h. Cells were lysed in buffer containing 50 mM Tris, pH 7.4, 150 mM NaCl, 1% Nonidet P-40, 2 mM ethylenediaminetetraacetic acid (EDTA), and protease inhibitors. The lysates were preadsorbed to A/G plus agarose (sc-2003, Santa Cruz Biotechnology, Inc.) at 4 °C for 1 h. Preadsorbed lysates were incubated with a specific primary antibody against β-catenin (610153, BD Biosciences) overnight at 4 °C. A/G Plus agarose was then added to the lysate mixture, which was then incubated for 3 h. The beads were washed 5 times with lysis buffer at 4 °C. The bound protein was eluted by boiling in SDS sample buffer and loaded onto an SDS−8% polyacrylamide gel for electrophoretic analysis. Separated proteins were transferred onto nitrocellulose membranes for immunoblot analysis. Antibodies against BCL9 (ab37305, Abcam) or E-cadherin (610404, BD Biosciences) were incubated with the membranes. IRDye 680LT goat anti-mouse IgG (827-11080, LiCOR) was used as the secondary antibody. Images were detected by the Odyssey infrared imaging system (LiCOR). Experiments were performed in duplicate.

MTS Cell Viability Assay. Colorectal cancer cell lines (SW480, HT29, and HCT116), triple-negative breast cancer cell lines (MDA-MB-231 and MDA-MB-436), lung adenocarcinoma cell line (A549), and normal mammary epithelial cell line (MCF10A) were seeded in 96-well plates at 4×10^3 cells/well, maintained overnight at 37 °C, and incubated in the presence of **21**, **22**, **23**, or carnosic acid at various concentrations. Cell viability was monitored after 72 h by use of a freshly prepared mixture of 1 part phenazine methosulfate (PMS, Sigma) solution (0.92 mg/mL) and 19 parts 3-(4,5-dimethylthiazol-2-yl)-5-(3-carboxymethoxyphenyl)-2-(4-sulfophenyl)-2*H*-tetrazolium (MTS, Promega) solution (2 mg/mL). Cells were incubated in 10 μL of this solution at 37 °C for 3 h, and A_{490} was measured. The effect of each compound is expressed as the concentration required to reduce A_{490} by 50% (IC_{50}) relative to vehicle-treated cells. Experiments were performed in triplicate.

Anchorage-Independent Growth Assay. Three milliliters of 0.5% agar in DMEM supplemented with 10% FBS was layered onto 6 cm tissue culture plates. HCT116 cells (5×10^3) treated with different concentrations of **22** were added to 0.35% agar in DMEM supplemented with 10% FBS, and the mixture was then added to the top of the 0.5% agar-precoated tissue culture plates. Cells were incubated at 37 °C in 5% CO_2 for 18 days, and the number of colonies was scored by crystal violet staining. Relative colony number was calculated as $[(\text{colony number})_{\text{treatment}}/(\text{colony number})_{\text{control}}] \times 100$. Each assay was performed in duplicate.

■ ASSOCIATED CONTENT

Supporting Information

The Supporting Information is available free of charge on the ACS Publications website at DOI: 10.1021/jacs.5b04988.

Conformational analysis of **1**, text and 12 schemes with synthetic procedures for **2**−**30**, HPLC conditions, Figures S1−S19 as described in the text, and one table listing results of PDB data mining (PDF)

^{1}H and ^{13}C NMR spectra for various compounds (PDF)

HPLC traces for **17**, **18**, **21**−**24**, and **27**−**30** (PDF)

■ AUTHOR INFORMATION

Corresponding Author

*markji@chem.utah.edu.

Author Contributions

†L.R.H. and Y.Z. contributed equally to this work.

Notes

The authors declare no competing financial interest.

■ ACKNOWLEDGMENTS

This work was in part supported by the Department of Defense CDMRP BCRP breakthrough award W81XWH-14-1-0083. We thank Dr. David P. Goldenberg at the University of Utah for use of his isothermal titration calorimetry instrument and the Center for High-Performance Computing at the University of Utah for computer time.

■ REFERENCES

(1) Milroy, L.-G.; Grossmann, T. N.; Hennig, S.; Brunsveld, L.; Ottmann, C. *Chem. Rev.* **2014**, *114*, 4695−4748.

(2) Clackson, T.; Wells, J. A. *Science* **1995**, *267*, 383−386.

(3) Guo, W.; Wisniewski, J. A.; Ji, H. *Bioorg. Med. Chem. Lett.* **2014**, *24*, 2546−2554.

(4) Arkin, M. R.; Tang, Y.; Wells, J. A. *Chem. Biol.* **2014**, *21*, 1102−1114.

(5) Bullock, B. N.; Jochim, A. L.; Arora, P. S. *J. Am. Chem. Soc.* **2011**, *133*, 14220−14223.

(6) Clevers, H.; Nusse, R. *Cell* **2012**, *149*, 1192−1205.

(7) Anastas, J. N.; Moon, R. T. *Nat. Rev. Cancer* **2013**, *13*, 11−26.

(8) Adachi, S.; Jigami, T.; Yasui, T.; Nakano, T.; Ohwada, S.; Omori, Y.; Sugano, S.; Ohkawara, B.; Shibuya, H.; Nakamura, T.; Akiyama, T. *Cancer Res.* **2004**, *64*, 8496−8501.

(9) de la Roche, M.; Worm, J.; Bienz, M. *BMC Cancer* **2008**, *8*, 199.

(10) Mani, M.; Carrasco, D. E.; Zhang, Y.; Takada, K.; Gatt, M. E.; Dutta-Simmons, J.; Ikeda, H.; Diaz-Griffero, F.; Pena-Cruz, V.; Bertagnolli, M.; Myeroff, L. L.; Markowitz, S. D.; Anderson, K. C.; Carrasco, D. R. *Cancer Res.* **2009**, *69*, 7577−7586.

(11) Brembeck, F. H.; Wiese, M.; Zatula, N.; Grigoryan, T.; Dai, Y.; Fritzmann, J.; Birchmeier, W. *Gastroenterology* **2011**, *141*, 1359−1370.

(12) Brembeck, F. H.; Schwarz-Romond, T.; Bakkers, J.; Wilhelm, S.; Hammerschmidt, M.; Birchmeier, W. *Genes Dev.* **2004**, *18*, 2225−2230.

(13) Zhao, J.-J.; Lin, J.; Zhu, D.; Wang, X.; Brooks, D.; Chen, M.; Chu, Z.-B.; Takada, K.; Ciccarelli, B.; Admin, S.; Tao, J.; Tai, Y.-T.; Treon, S.; Pinkus, G.; Kuo, W. P.; Hideshima, T.; Bouxsein, M.; Munshi, N.; Anderson, K.; Carrasco, R. *Cancer Res.* **2014**, *74*, 1801−1813.

(14) Sampietro, J.; Dahlberg, C. L.; Cho, U. S.; Hinds, T. R.; Kimelman, D.; Xu, W. *Mol. Cell* **2006**, *24*, 293−300.

(15) Kawamoto, S. A.; Coleska, A.; Ran, X.; Yi, H.; Yang, C.-Y.; Wang, S. *J. Med. Chem.* **2012**, *55*, 1137−1146.

(16) Takada, K.; Zhu, D.; Bird, G. H.; Sukhdeo, K.; Zhao, J.-J.; Mani, M.; Lemieux, M.; Carrasco, D. E.; Ryan, J.; Horst, D.; Fulciniti, M.; Munshi, N. C.; Xu, W.; Kung, A. L.; Shivdasani, R. A.; Walensky, L. D.; Carrasco, D. R. *Sci. Transl. Med.* **2012**, *4*, 148ra117.

(17) de la Roche, M.; Rutherford, T. J.; Gupta, D.; Veprintsev, D. B.; Saxty, B.; Freund, S. M.; Bienz, M. *Nat. Commun.* **2012**, *3*, 680.

(18) Baell, J. B.; Holloway, G. A. *J. Med. Chem.* **2010**, *53*, 2719−2740.

(19) Baell, J.; Walters, M. A. *Nature* **2014**, *513*, 481−483.

(20) Jochim, A. L.; Arora, P. S. *Mol. BioSyst.* **2009**, *5*, 924−926.

(21) Jochim, A. L.; Arora, P. S. *ACS Chem. Biol.* **2010**, *5*, 919−923.

(22) Bergey, C. M.; Watkins, A. M.; Arora, P. S. *Bioinformatics* **2013**, *29*, 2806−2807.

(23) Teuscher, K. B.; Ji, H. *Methods Mol. Biol.* **2015**, *1289*, 57−73.

(24) Yu, B.; Huang, Z.; Zhang, M.; Dillard, D. R.; Ji, H. *ACS Chem. Biol.* **2013**, *8*, 524−529.

(25) Ji, H.; Stanton, B. Z.; Igarashi, J.; Li, H.; Martásek, P.; Roman, L. J.; Poulos, T. L.; Silverman, R. B. *J. Am. Chem. Soc.* **2008**, *130*, 3900−3914.

(26) Ji, H.; Li, H.; Martásek, P.; Roman, L. J.; Poulos, T. L.; Silverman, R. B. *J. Med. Chem.* **2009**, *52*, 779−797.

(27) Smits, C.; Czabotar, P. E.; Hinds, M. G.; Day, C. L. *Structure* **2008**, *16*, 818−829.

(28) Jiao, L.; Ouyang, S.; Liang, M.; Niu, F.; Shaw, N.; Wu, W.; Ding, W.; Jin, C.; Peng, Y.; Zhu, Y.; Zhang, F.; Wang, T.; Li, C.; Zuo, X.; Luan, C.-H.; Li, D.; Liu, Z.-J. *J. Virol.* **2013**, *87*, 6829−6839.

DOI: 10.1021/jacs.5b04988
J. Am. Chem. Soc. 2015, 137, 12249−12260

(29) Grigoriu, S.; Bond, R.; Cossio, P.; Chen, J. A.; Ly, N.; Hummer, G.; Page, R.; Cyert, M. S.; Peti, W. *PLoS Biol.* **2013**, *11*, e1001492.
(30) Hoffmans, R.; Basler, K. *Development* **2004**, *131*, 4393−4400.
(31) Hoffmans, R.; Basler, K. *Mech. Dev.* **2007**, *124*, 59−67.
(32) Valenta, T.; Gay, M.; Steiner, S.; Draganova, K.; Zemke, M.; Hoffmans, R.; Cinelli, P.; Aguet, M.; Sommer, L.; Basler, K. *Genes Dev.* **2011**, *25*, 2631−2643.
(33) Kawamoto, S. A.; Thompson, A. D.; Coleska, A.; Nikolovska-Coleska, Z.; Yi, H.; Wang, S. *Biochemistry* **2009**, *48*, 9534−9541.
(34) Zhang, M.; Wisniewski, J. A.; Ji, H. *Anal. Biochem.* **2015**, *469*, 43−53.
(35) Morris, G. M.; Huey, R.; Lindstrom, W.; Sanner, M. F.; Belew, R. K.; Goodsell, D. S.; Olson, A. J. *J. Comput. Chem.* **2009**, *30*, 2785−2791.
(36) Friesner, R. A.; Murphy, R. B.; Repasky, M. P.; Frye, L. L.; Greenwood, J. R.; Halgren, T. A.; Sanschagrin, P. C.; Mainz, D. T. *J. Med. Chem.* **2006**, *49*, 6177−6196.
(37) Huber, A. H.; Weis, W. I. *Cell* **2001**, *105*, 391−402.
(38) Choi, H.-J.; Huber, A. H.; Weis, W. I. *J. Biol. Chem.* **2006**, *281*, 1027−1038.
(39) Choi, H.-J.; Gross, J. C.; Pokutta, S.; Weis, W. I. *J. Biol. Chem.* **2009**, *284*, 31776−3188.
(40) Zhang, M.; Catrow, J. L.; Ji, H. *ACS Med. Chem. Lett.* **2013**, *4*, 306−311.
(41) Staal, F. J. T.; van Noort, M.; Strous, G. J.; Clevers, H. C. *EMBO Rep.* **2002**, *3*, 63−68.
(42) Walensky, L. D.; Bird, G. H. *J. Med. Chem.* **2014**, *57*, 6275−6288.
(43) Patgiri, A.; Jochim, A. L.; Arora, P. S. *Acc. Chem. Res.* **2008**, *41*, 1289−1300.
(44) Cheng, R. P.; Gellman, S. H.; DeGrado, W. F. *Chem. Rev.* **2001**, *101*, 3219−3232.
(45) Orner, B. P.; Ernst, J. T.; Hamilton, A. D. *J. Am. Chem. Soc.* **2001**, *123*, 5382−5383.
(46) Kutzki, O.; Park, H. S.; Ernst, J. T.; Orner, B. P.; Yin, H.; Hamilton, A. D. *J. Am. Chem. Soc.* **2002**, *124*, 11838−11839.
(47) Kazi, A.; Sun, J.; Doi, K.; Sung, S.-S.; Takahashi, Y.; Yin, H.; Rodriguez, J. M.; Becerril, J.; Berndt, N.; Hamilton, A. D.; Wang, H.-G.; Sebti, S. M. *J. Biol. Chem.* **2011**, *286*, 9382−9392.
(48) Yin, H.; Lee, G.-i.; Park, H. S.; Payne, G. A.; Rodriguez, J. M.; Sebti, S. M.; Hamilton, A. D. *Angew. Chem., Int. Ed.* **2005**, *44*, 2704−2707.
(49) Davis, J. M.; Truong, A.; Hamilton, A. D. *Org. Lett.* **2005**, *7*, 5405−5408.
(50) Volonterio, A.; Moisan, L.; Rebek, J., Jr. *Org. Lett.* **2007**, *9*, 3733−3736.
(51) Maity, P.; König, B. *Org. Lett.* **2008**, *10*, 1473−1476.
(52) Lao, B. B.; Drew, K.; Guarracino, D. A.; Brewer, T. F.; Heindel, D. W.; Bonneau, R.; Arora, P. S. *J. Am. Chem. Soc.* **2014**, *136*, 7877−7888.
(53) Yin, H.; Lee, G.-i.; Sedey, K. A.; Rodriguez, J. M.; Wang, H.-G.; Sebti, S. M.; Hamilton, A. D. *J. Am. Chem. Soc.* **2005**, *127*, 5463−5468.
(54) Rodriguez, J. M.; Hamilton, A. D. *Angew. Chem., Int. Ed.* **2007**, *46*, 8614−8617.
(55) Shaginian, A.; Whitby, L. R.; Hong, S.; Hwang, I.; Farooqi, B.; Searcey, M.; Chen, J.; Vogt, P. K.; Boger, D. L. *J. Am. Chem. Soc.* **2009**, *131*, 5564−5572.
(56) Shahian, T.; Lee, G. M.; Lazic, A.; Arnold, L. A.; Velusamy, P.; Roels, C. M.; Guy, R. K.; Craik, C. S. *Nat. Chem. Biol.* **2009**, *5*, 640−646.
(57) Ravindranathan, P.; Lee, T.-K.; Yang, L.; Centenera, M. M.; Butler, L.; Tilley, W. D.; Hsieh, J.-T.; Ahn, J.-M.; Raj, G. V. *Nat. Commun.* **2013**, *4*, 1923.
(58) Hebda, J. A.; Saraogi, I.; Magzoub, M.; Hamilton, A. D.; Miranker, A. D. *Chem. Biol.* **2009**, *16*, 943−950.
(59) Saraogi, I.; Hebda, J. A.; Becerril, J.; Estroff, L. A.; Miranker, A. D.; Hamilton, A. D. *Angew. Chem., Int. Ed.* **2010**, *49*, 736−739.
(60) Lee, J. H.; Zhang, Q.; Jo, S.; Chai, S. C.; Oh, M.; Im, W.; Lu, H.; Lim, H.-S. *J. Am. Chem. Soc.* **2011**, *133*, 676−679.
(61) Oh, M.; Lee, J. H.; Wang, W.; Lee, H. S.; Lee, W. S.; Burlak, C.; Im, W.; Hoang, Q. Q.; Lim, H.-S. *Proc. Natl. Acad. Sci. U. S. A.* **2014**, *111*, 11007−11012.
(62) Azzarito, V.; Long, K.; Murphy, N. S.; Wilson, A. J. *Nat. Chem.* **2013**, *5*, 161−173.
(63) Barnard, A.; Long, K.; Martin, H. L.; Miles, J. A.; Edwards, T. A.; Tomlinson, D. C.; Macdonald, A.; Wilson, A. J. *Angew. Chem., Int. Ed.* **2015**, *54*, 2960−2965.
(64) Vassilev, L. T.; Vu, B. T.; Graves, B.; Carvajal, D.; Podlaski, F.; Filipovic, Z.; Kong, N.; Kammlott, U.; Lukacs, C.; Klein, C.; Fotouhi, N.; Liu, E. A. *Science* **2004**, *303*, 844−848.
(65) Grasberger, B. L.; Lu, T.; Schubert, C.; Parks, D. J.; Carver, T. E.; Koblish, H. K.; Cummings, M. D.; LaFrance, L. V.; Milkiewicz, K. L.; Calvo, R. R.; Maguire, D.; Lattanze, J.; Franks, C. F.; Zhao, S.; Ramachandren, K.; Bylebyl, G. R.; Zhang, M.; Manthey, C. L.; Petrella, E. C.; Pantoliano, M. W.; Deckman, I. C.; Spurlino, J. C.; Maroney, A. C.; Tomczuk, B. E.; Molloy, C. J.; Bone, R. F. *J. Med. Chem.* **2005**, *48*, 909−912.
(66) Ding, K.; Lu, Y.; Nikolovska-Coleska, Z.; Qiu, S.; Ding, Y.; Gao, W.; Stuckey, J.; Krajewski, K.; Roller, P. P.; Tomita, Y.; Parrish, D. A.; Deschamps, J. R.; Wang, S. *J. Am. Chem. Soc.* **2005**, *127*, 10130−10131.
(67) Zhang, Z.; Li, X.; Song, T.; Zhao, Y.; Feng, Y. *J. Med. Chem.* **2012**, *55*, 10735−10741.
(68) Ko, E.; Raghuraman, A.; Perez, L. M.; Ioerger, T. R.; Burgess, K. *J. Am. Chem. Soc.* **2013**, *135*, 167−173.
(69) Armbruster, C.; Vorbach, H.; Steindl, F.; El Menyawi, I. *J. Antimicrob. Chemother.* **2001**, *47*, 487−490.
(70) Colletti, L. M.; Liu, Y.; Koev, G.; Richardson, P. L.; Chen, C.-M.; Kati, W. *Anal. Biochem.* **2008**, *383*, 186−193.
(71) Huang, Z.; Zhang, M.; Burton, S. D.; Katsakhyan, L. N.; Ji, H. *ACS Chem. Biol.* **2014**, *9*, 193−201.
(72) Catrow, J. L.; Zhang, Y.; Zhang, M.; Ji, H. *J. Med. Chem.* **2015**, *58*, 4678−4692.

DOI: 10.1021/jacs.5b04988
J. Am. Chem. Soc. 2015, 137, 12249−12260